Synthesis and Characterization of Stable and Crystalline $Ce_{1-x}Zr_xO_2$ Nanoparticle Sols

Atul S. Deshpande,[†] Nicola Pinna,[†] Pablo Beato,[‡] Markus Antonietti,[†] and Markus Niederberger*[,†]

Colloid Chemistry, Max-Planck-Institute of Colloids and Interfaces, D-14424 Potsdam, Germany, and Department of Inorganic Chemistry, Fritz-Haber-Institute of the Max-Planck-Society, Faradayweg 4−6, D-14195 Berlin, Germany

Received March 2, 2004. Revised Manuscript Received April 8, 2004

$Ce_{1-x}Zr_xO_2$ nanoparticle sols ($x = 0-1$) are synthesized by hydroxide coprecipitation of a mixed precursor solution of cerium ammonium nitrate and zirconyl chloride followed by redispersion in an aqueous medium by sonication using nitric acid as the peptizing agent. The obtained sols are highly concentrated and stable for weeks. Analytical ultracentrifugation measurements show a particularly narrow particle distribution with an average particle size of about 3.5 nm for pure CeO_2 and 2.5 nm for pure ZrO_2 nanoparticles. Wide-angle X-ray scattering (XRD) as well as high-resolution transmission electron microscopy give evidence that all of the as-synthesized nanoparticle sols with a ceria content larger than 20 mol % are well crystalline. The formation of a solid solution with an increasing amount of Zr was monitored by XRD and Raman spectroscopy.

Introduction

CeO_2-based materials have earned a great amount of interest in the field of catalysis because of properties such as thermal stability, oxygen storage capacity, promotion of water gas shift and reforming reaction, noble metal dispersion, etc. In the past decade, researchers in the areas of automotive exhaust catalyst and solid oxide fuel cells have extensively tested the potential of CeO_2-based materials and reached a general conclusion that "CeO_2 is good!".[1] A great deal of literature is available on ceria- and CeO_2-based systems, and the pool of knowledge is expanding at a constant rate.[1−4]

A large number of reports can be found on the synthesis of nanoparticles of CeO_2-based materials. Nanoparticles offer an attractive way for conventional applications such as coatings,[5] thin films,[6,7] and active powders for low-temperature sintering,[8] while newer synthetic strategies for fabrication of nanostructured materials via the templating process[9] and nanotectonic[10] approach depict the usefulness of nanoparticles as nano building blocks. In general, all of these applications demand certain features such as monodispersity and nonagglomeration to have the nanoparticles as sols in a suitable solvent. When it comes to doped or binary systems such as CeO_2-ZrO_2, additional parameters such as compositional homogeneity come into the picture. Most of the methods reported on the synthesis of CeO_2-based nanoparticles are based on forced hydrolysis from a metal precursor solution,[11] hydrothermal processes,[12,13] coprecipitation,[14,15] flame pyrolysis,[16] or emulsion,[17−19] and yield powders rather than stable suspensions or sols. Spalla et al. reported the synthesis and detailed characterization of CeO_2 nanoparticles.[20,21] Apart from that, there are only a few reports where the synthesis of CeO_2 or CeO_2-ZrO_2 nanoparticle sols has been mentioned.[6,9,22] However, they have certain drawbacks such as polydispersity and destabilization in aqueous media. In the case of Shchukin et al., the

* Corresponding author. E-mail: Markus.Niederberger@mpikg-golm.mpg.de.
[†] Max-Planck-Institute of Colloids and Interfaces.
[‡] Fritz-Haber-Institute of the Max-Planck-Society.

(1) Kaspar, J.; Fornasiero, P.; Graziani, M. *Catal. Today* **1999**, *50*, 285−298.
(2) Trovarelli, A. *Catal. Rev.−Sci. Eng.* **1996**, *38*, 439−520.
(3) Kaspar, J.; Fornasiero, P.; Hickey, N. *Catal. Today* **2003**, *77*, 419−449.
(4) Kaspar, J.; Fornasiero, P. *J. Solid State Chem.* **2003**, *171*, 19−29.
(5) Patil, S.; Kuiry, S. C.; Seal, S.; Vanfleet, R. *J. Nanopart. Res.* **2002**, *4*, 433−438.
(6) Luo, X.; Zhu, B.; Xia, C.; Niklasson, G. A.; Granqvist, C. G. *Sol. Energy Mater. Sol. Cells* **1998**, *53*, 341−347.
(7) Masui, T.; Yamamoto, M.; Sakata, T.; Mori, H.; Adachi, G. *J. Mater. Chem.* **2000**, *10*, 353−357.
(8) Chen, P. L.; Chen, I. W. *J. Am. Ceram. Soc.* **1993**, *76*, 1577−1583.
(9) Shchukin, D. G.; Caruso, R. A. *Adv. Funct. Mater.* **2003**, *13*, 789−794.
(10) Bouchara, A.; Soler-Illia, G.; Chane-Ching, J. Y.; Sanchez, C. *Chem. Commun.* **2002**, 1234−1235.
(11) Hirano, M.; Miwa, T.; Inagaki, M. *J. Solid State Chem.* **2001**, *158*, 112−117.
(12) Cabanas, A.; Darr, J. A.; Lester, E.; Poliakoff, M. *Chem. Commun.* **2000**, 901−902.
(13) Hirano, M.; Hirai, K. *J. Nanopart. Res.* **2003**, *5*, 147−156.
(14) Kaspar, J.; Fornasiero, P.; Baiducci, G.; Di Monte, R.; Hickey, N.; Sergo, V. *Inorg. Chim. Acta* **2003**, *349*, 217−226.
(15) Li, J. G.; Ikegami, T.; Wang, Y. R.; Mori, T. *J. Solid State Chem.* **2002**, *168*, 52−59.
(16) Stark, W. J.; Maciejewski, M.; Madler, L.; Pratsinis, S. E.; Baiker, A. *J. Catal.* **2003**, *220*, 35−43.
(17) Zhang, J.; Ju, X.; Wu, Z. Y.; Liu, T.; Hu, T. D.; Xie, Y. N.; Zhang, Z. L. *Chem. Mater.* **2001**, *13*, 4192−4197.
(18) Manziek, L.; Langenmayr, E.; Lamola, A.; Gallagher, M.; Brese, N.; Annan, N. *Chem. Mater.* **1998**, *10*, 3101−3108.
(19) He, Y. J.; Yang, B. L.; Cheng, C. X. *Mater. Lett.* **2003**, *57*, 1880−1884.
(20) Nabavi, M.; Spalla, O.; Cabane, B. *J. Colloid Interface Sci.* **1993**, *160*, 459−471.
(21) Spalla, O.; Kekicheff, P. *J. Colloid Interface Sci.* **1997**, *192*, 43−65.

10.1021/cm040155w CCC: $27.50
Published on Web 05/28/2004

reported synthesis of CeO_2 and ZrO_2 nanoparticles[9] results in the formation of amorphous materials. Furthermore, to the best of our knowledge, there are no reports on the synthesis of the complete range of $Ce_{1-x}Zr_xO_2$ nanoparticle sols ($x = 0-1$). We report here the synthesis of surfactant-free and crystalline $Ce_{1-x}Zr_xO_2$ nanoparticle sols ($x = 0-1$) with a particularly narrow size distribution. The sols were characterized in detail by wide-angle X-ray scattering (XRD), high-resolution transmission electron microscopy (HRTEM), analytical ultracentrifugation (AUC), and Raman spectroscopy.

Results and Discussion

During the synthesis of the $Ce_{1-x}Zr_xO_2$ sols, the first step was the hydrolysis of the mixed precursor by addition of an aqueous NH_3 solution resulting in a pH higher than 10. It was necessary to wash off the excess of base immediately after the precipitation process. We observed that aging of the precipitate in a basic medium, even for less than an hour, failed to give a transparent sol. The small solubility product of 2×10^{-48} and the basic behavior of $Ce(OH)_4$ lead to the situation that an increase of the pH decreases the solubility of $Ce(OH)_4$, whereas a decrease of the pH increases the solubility.[23] Accordingly, at basic pH the Ostwald ripening process enhances the growth of large particles, because precipitated $Ce(OH)_4$ clusters contribute to the crystal growth, whereas smaller grains dissolve slowly. After the washing step, nitric acid was added and the suspension was sonicated. The addition of acid leads to the opposite situation, namely, a decrease of the pH, so that smaller hydroxide particles dissolve fast and that the larger ones grow slowly because of the low $Ce(OH)_4$ concentration. Sonication enhanced this process and prevented the growth of particles beyond a certain extent by breaking up the larger agglomerates. The particle surface is covered with hydroxyl groups. Because the pH of the sol was below 2, some of the hydroxyls are protonated, leading to positively charged particles. The positive charge is counterbalanced by nitrate anions forming the Stern layer.[20,21] This imparts stability to the nanoparticles in the sol. The sols do not undergo gelation or sedimentation for at least 12 weeks. Upon dialysis of the sol to a pH of 4−5, it started to gel slowly over a period of 1−2 days. Depending on the starting composition, the solid content in the sols was about 5−8 wt %. Undialyzed sols were found to be stable on the addition of a large quantity of alcohol. The sols that were dialyzed against ethanol showed that about 90% of water could be replaced by ethanol. However, total water replacement was not possible and resulted in precipitation of nanoparticles.

For many applications of nanoparticles, the particle size distribution is a fundamental parameter, but still its determination often remains a difficult task. Although literature reports generally present particle size distribution data, based on TEM results,[22,24] there are no unambiguous statistics for the particle size distribution of the whole sample. AUC has proven to be a versatile tool for the measurement of the particle size distribution of colloidal samples.[25,26] In contrast to TEM, AUC detects all particles even down to the smallest sizes. The resolution of the particle size distribution for small nanoparticles lies in the sub-Angström range.[27]

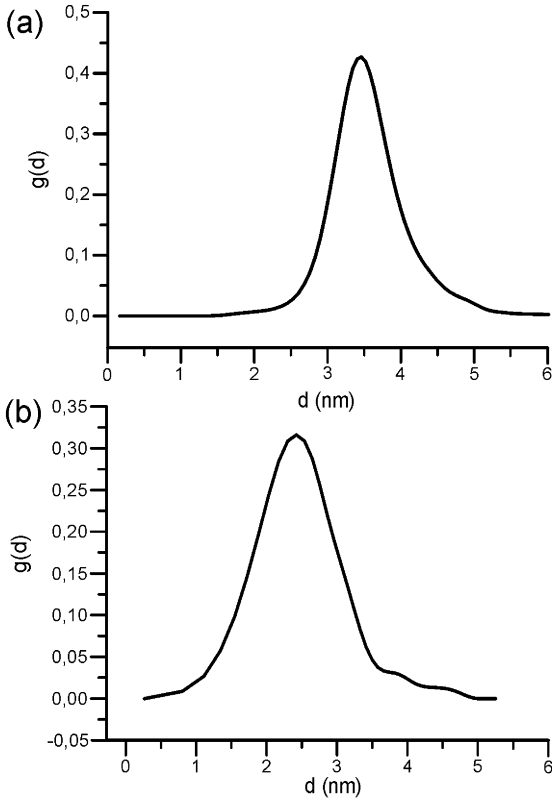

Figure 1. Particle size distribution (volume-weighted) curves for dialyzed CeO_2 (a) and ZrO_2 sol (b) obtained by AUC analysis.

The AUC experiments were performed at 40 000 and 60 000 rpm for dialyzed CeO_2 and ZrO_2 sols, respectively, using a 675 nm laser and interference optics. Figure 1 shows the particle size distribution (volume weighted) for pure CeO_2 (a) and ZrO_2 sols (b). For both samples, the particle size distribution is particularly narrow. It has to be noted that this particle size distribution is even broader than the real one because diffusive peak broadening is not corrected. For CeO_2, the average particle diameter was 3.5 nm and for ZrO_2 2.5 nm. No other signals were obtained at slower rotation speeds, indicating that the particles were nonaggregated.

Powder XRD patterns of dried gels are shown in Figure 2. The patterns are named according to the CeO_2 content of the sample; i.e., Ce-100 contains 100 mol % Ce. All of the samples, except the pure ZrO_2 (Ce-00) and the 10 mol % CeO_2 (Ce-10), show broad reflections corresponding to the cubic fluorite type phase. The Ce-00 sample displays only two humps, indicating that the sample is X-ray amorphous. Although the Ce-10 sample shows weak reflections of the cubic fluorite structure,

(22) Tsunekawa, S.; Sivamohan, R.; Ohsuna, T.; Kasuya, A.; Takahashi, H.; Tohji, K. *Materials Science Forum—Rare Earths '98*; Transtec Publications Ltd.: Zurich-Uetikon, 1999; Vol. 315-3, pp 439−445.
(23) Wu, N. C.; Shi, E. W.; Zheng, Y. Q.; Li, W. J. *J. Am. Ceram. Soc.* **2002**, *85*, 2462−2468.
(24) Wang, H.; Zhu, J. J.; Zhu, J. M.; Liao, X. H.; Xu, S.; Ding, T.; Chen, H. Y. *Phys. Chem. Chem. Phys.* **2002**, *4*, 3794−3799.
(25) Svedberg, T.; Rinde, H. *J. Am. Chem. Soc.* **1923**, *45*, 943−954.
(26) Svedberg, T.; Pedersen, K. O. *The Ultracentrifuge*; Clarendon Press: Oxford, U.K., 1940.
(27) Cölfen, H.; Pauck, T. *Colloid Polym. Sci.* **1997**, *275*, 175−180.

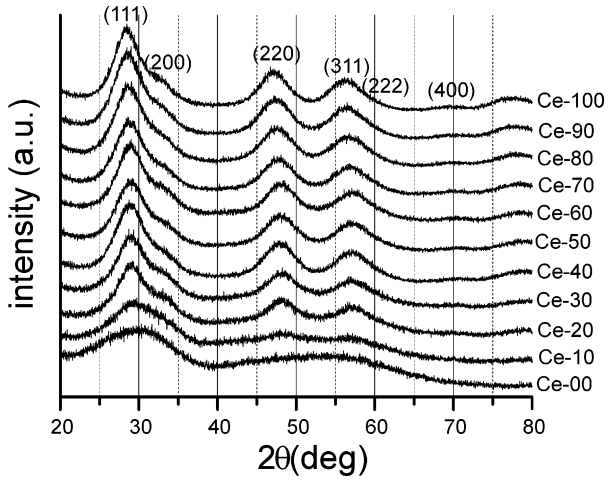

Figure 2. XRD patterns of gels obtained from the dialyzed sols.

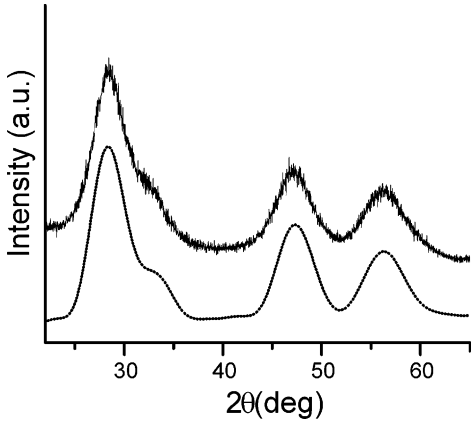

Figure 3. Calculated diffraction patterns for spherical, monodisperse CeO_2 cubic nanoparticles with a diameter of 2.5 nm (dotted line) and an experimental pattern (full line) of CeO_2 nanoparticles.

the sample is still predominantly amorphous. According to the Scherrer equation, the average particle size calculated from the (220) reflection is approximately 2.5 nm for Ce-100, and with increasing zirconia content, the crystallite sizes become smaller. Figure 3 displays the experimental powder XRD pattern of the Ce-100 sample (Figure 3, full line) together with the XRD pattern calculated by the Debye equation of kinematic diffraction for spherical, monodisperse particles of 2.5 nm diameter with the cubic fluorite structure (Figure 3, dotted line).[28,29] The calculated and experimental patterns match well. Assuming that all of the particles are monocrystalline, the discrepancy in the average particle diameter obtained from AUC analysis and from XRD data may be due to the difference in the diameter of the dried particles and the particles in solution. As discussed before, in the stabilized sols, the particles possess a layer of tightly bound ionic double layers (Stern layer) followed by a solvent molecules depleted ionic layer, which makes the radius larger in the AUC analysis than the actual particle size.[30]

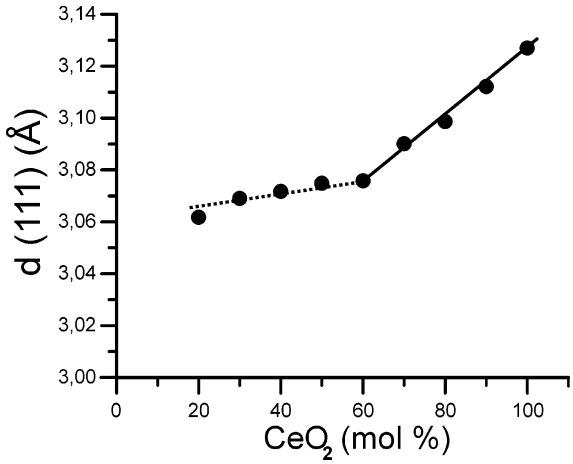

Figure 4. Variation of the *d* value of the (111) reflection with the CeO_2 content.

The phase diagram for the CeO_2-ZrO_2 system reported in the literature depicts three major phases, i.e., cubic, tetragonal, and monoclinic. The tetragonal phase is further divided into stable *t* and metastable *t′* and *t″* structures.[1,31,32] In the case of the formation of a solid solution between CeO_2 and ZrO_2, the smaller Zr^{4+} (ionic radius = 0.84 Å) occupies the position of the larger Ce^{4+} (ionic radius = 0.97 Å). According to Vegard's rule, a decrease in the cell volume is expected for both the cubic and tetragonal phases with an increase in the ZrO_2 content. Even though XRD is not sensitive enough to distinguish between the cubic *t′* and *t″* phases, especially in the case of poorly crystalline and/or very small particles, the correlation between the *d* values for the (111) reflection in dependence of the CeO_2 content gives a hint about phase changes[33] (Figure 4). The decrease in the *d* values with a decrease in the CeO_2 mole percent confirms the formation of a solid solution in the system. In addition, there is a linear decrease of the *d* values from Ce-100 to Ce-60 representing the cubic phase structure. From Ce-50 to Ce-20, the *d* values change only slightly. This composition range corresponds to the cubic *t′* and *t″* mixed-phase region as discussed by Vlaic et al.[33] The lattice parameter calculated from the (111) reflection of the pure CeO_2 sample is $a = 5.42$ Å, which matches well with the lattice parameter of bulk CeO_2 oxide ($a = 5.411\ 34$).[34] It was reported for CeO_2 nanoparticles that because of the presence of oxygen deficiency and lattice defects the lattice parameter increases with decreasing particle size.[35,36] However, despite the small particle size of 2.5 nm, practically no difference of the lattice parameters between the nanoparticulate and the bulk phase is found. Because the experimental XRD pattern matches perfectly with the one calculated by the Debye equation of kinematic diffraction for defect-free particles of 2.5 nm diameter, it is reasonable to conclude that the as-synthesized nanoparticles are

(28) Pinna, N.; Wild, U.; Urban, J.; Schlogl, R. *Adv. Mater.* **2003**, *15*, 329−331.
(29) Vogel, W. *Cryst. Res. Technol.* **1998**, *33*, 1141−1154.
(30) Kurth, D. G.; Lehmann, P.; Volkmer, D.; Colfen, H.; Koop, M. J.; Muller, A.; Du Chesne, A. *Chem. Eur. J.* **2000**, *6*, 385−393.
(31) Yashima, M.; Arashi, H.; Kakihana, M.; Yoshimura, M. *J. Am. Ceram. Soc.* **1994**, *77*, 1067−1071.
(32) Yashima, M.; Takashina, H.; Kakihana, M.; Yoshimura, M. *J. Am. Ceram. Soc.* **1994**, *77*, 1869−1874.
(33) Vlaic, G.; Di Monte, R.; Fornasiero, P.; Fonda, E.; Kaspar, J.; Graziani, M. *J. Catal.* **1999**, *182*, 378−389.
(34) JCPDS card number 43-1002.
(35) Tsunekawa, S.; Sivamohan, R.; Ito, S.; Kasuya, A.; Fukuda, T. *Nanostruct. Mater.* **1999**, *11*, 141−147.
(36) Tsunekawa, S.; Ishikawa, K.; Li, Z. Q.; Kawazoe, Y.; Kasuya, A. *Phys. Rev. Lett.* **2000**, *85*, 3440−3443.

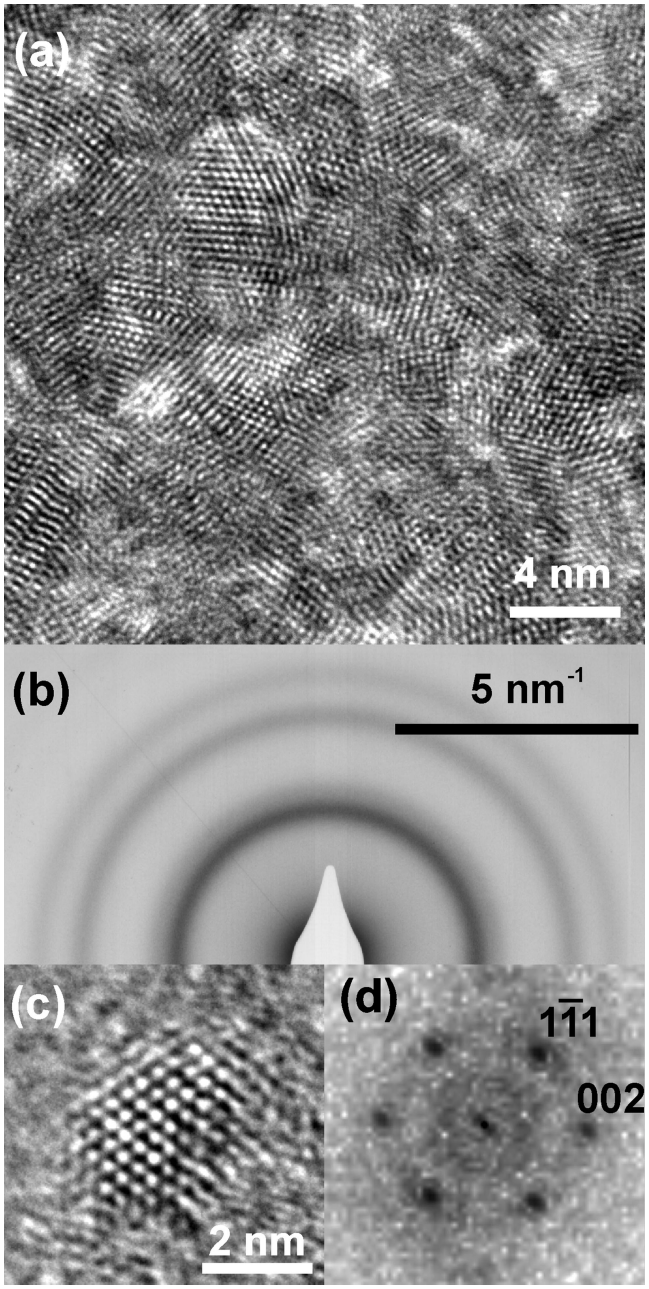

Figure 5. HRTEM image of an assembly of CeO_2 nanoparticles (a), SAED (b), HRTEM of an isolated particle (c), and respective PS (d).

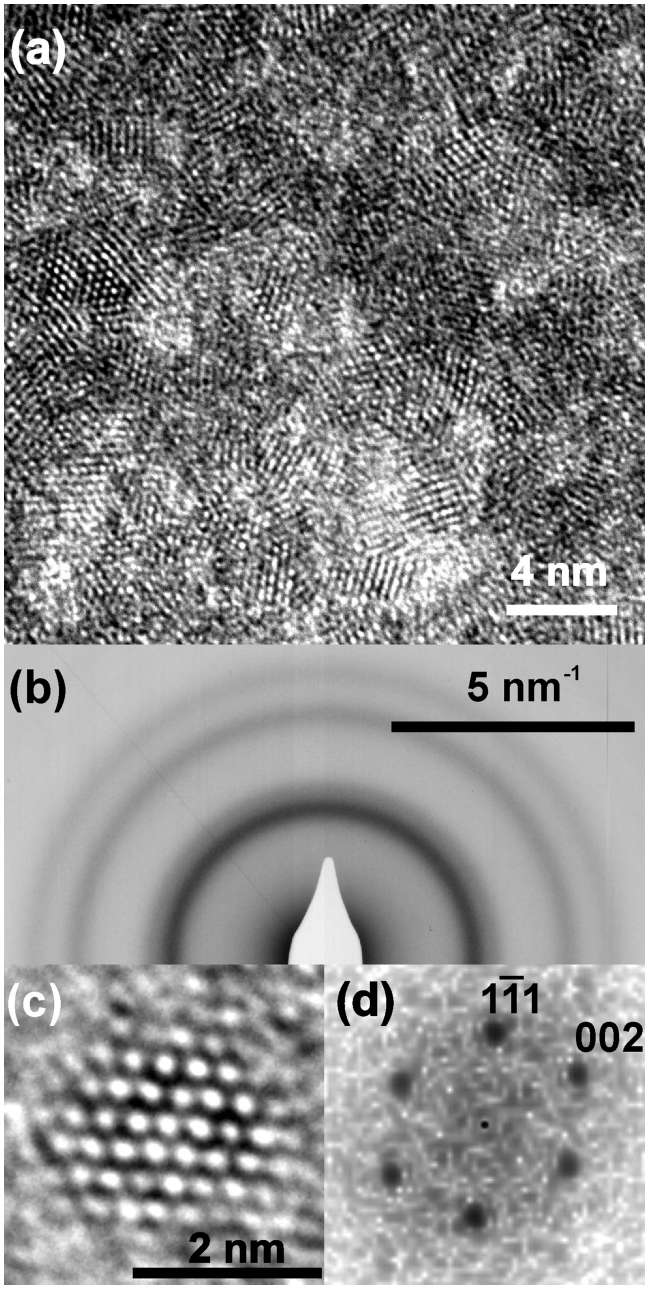

Figure 6. HRTEM image of an assembly of $Ce_{0.5}Zr_{0.5}O_2$ nanoparticles (a), SAED (b), HRTEM of an isolated particle (c), and respective PS (d).

stoichiometric and nearly free of lattice defects (cf. Figure 3).

Figure 5a shows a HRTEM image of an assembly of CeO_2 nanocrystals, exhibiting an average particle size of 2−3 nm. This agrees well with the experimental and calculated XRD powder patterns (cf. Figure 3). The lack of any surface protection layers results in some agglomeration of the particles. According to the randomly oriented lattice fringes, the particles are not coalesced. In Figure 5b, selected area electron diffraction (SAED) is presented. The lattice distances measured from the diffraction rings are in perfect agreement with the cubic fluorite structure of CeO_2. Figure 5c shows the HRTEM image of an isolated 2.5 nm particle oriented along the [110] direction. The power spectrum (PS; i.e., the square of the Fourier transform of the TEM image) of this particle is displayed in Figure 5d, giving evidence that the particles are well crystalline in the cubic fluorite structure without the presence of defaults.

Figure 6a shows a HRTEM image of an assembly of $Ce_{0.5}Zr_{0.5}O_2$ nanoparticles with a diameter of 2−3 nm. As for the pure CeO_2 nanocrystals, the particles are packed together but are not coalesced. The SAED pattern of one such spherical assembly (Figure 6b) shows broad rings that match with the $Ce_{0.5}Zr_{0.5}O_2$ structure. The HRTEM image of an isolated 2 nm particle proves the high crystallinity (Figure 6c). This is further confirmed by the PS of this particle (Figure 6d), which is characteristic for the $Ce_{0.5}Zr_{0.5}O_2$ structure without structural defaults. The particle is aligned along the [110] direction.

XRD, TEM, and HRTEM studies performed on the ZrO_2 particles show that they are smaller than 2 nm and mainly amorphous in nature. Raman spectroscopy

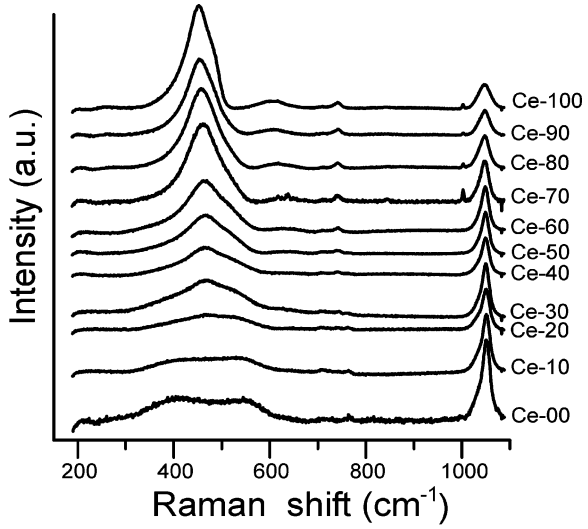

Figure 7. Raman spectra of gels obtained from the dialyzed sols.

was used to probe the local structure. Figure 7 depicts the Raman spectra of all samples. For Ce-00 (pure ZrO_2), two broad bands are observed at around 550 and 400 cm^{-1}. These two positions do not match with any of the standard Raman shifts reported for monoclinic, tetragonal, or cubic ZrO_2 structures. However, quite similar types of Raman spectra have previously been reported for pure zirconia gels prepared from zirconyl chloride.[37] The bands were attributed to polymeric Zr−O−Zr bonds in amorphous $ZrO_2 \cdot nH_2O$. The addition of 10 mol % CeO_2 in the Ce-10 sample induces a slight increase in the particle size. Even though the Ce-10 sample shows weak reflections in the XRD, according to the Raman spectrum, the local structure remains mainly disordered. A broad band appears around 470 cm^{-1} in the Ce-20 sample. With an increase in the CeO_2 content, the intensity of this band is increasing, while the bands around 550 and 400 cm^{-1} start to disappear. For higher CeO_2-containing samples (Ce-60 to Ce-100), a single broad band is observed, which can be attributed to the F_{2g} mode of the cubic fluorite structure. The continuous shift in the band position toward lower wavelength values with an increase in the CeO_2 content is in agreement with the increase in the lattice parameter observed by XRD. For cubic CeO_2 bulk material, a single symmetrical band around 465 cm^{-1} is reported in the literature.[31,38] Because the lattice parameter measured by XRD matches that of the bulk material, a corresponding symmetrical Raman band is expected. However, in the case of the pure CeO_2 sample (Ce-100), an asymmetrical band is found at 452 cm^{-1} instead of at 465 cm^{-1}. A possible explanation is the occurrence of a phonon confinement effect, frequently observed for nanocrystalline material.[39] The asymmetry, shift, or even appearance of new bands is explained by a relaxation of the $q = 0$ selection rule. This relaxation makes it possible to detect phonons from areas other than the center of the Brillouin zone. Another possible explanation lies in the fact that XRD essentially gives information on the periodicity of a material, while Raman spectroscopy depicts the vibrational behavior. The atoms on the surface are coordinatively unsaturated and hence show lower vibrational absorption than the bulk material. In the case of nanoparticles with sizes as small as 2.5 nm, the number of atoms at the surface is significantly higher than that inside the particle, resulting in a shift in the band position. The asymmetry could arise from the difference in absorption frequencies of atoms inside and on the surface of the particle.

In addition, in all of the samples, Raman shifts at 1050 and 700−750 cm^{-1} are observed, which are attributed to surface-bound nitrate groups.[40] Interestingly, for the samples Ce-100 to Ce-70, a small sharp band around 1000 cm^{-1} appears, which has not been reported previously. Generally, group V oxides exhibit such a Raman shift corresponding to terminal metal−oxygen double bonds (M═O).[41] These samples also show a weak shoulder around 600 cm^{-1}, which can be attributed to the presence of oxygen vacancies or lattice defects. However, the intensity of this shoulder is very low, indicating that there are almost no lattice defects present in the nanoparticles.

For the cubic structure a single band corresponding to the F_{2g} mode and for the tetragonal structure six bands related to one A_{1g}, three E_g, and two B_{1g} modes are expected. The Raman spectra of the Ce-50 to Ce-00 samples give no indication for the presence of the tetragonal structure. However, the broadness of the Raman shift as well as the absence of bands due to the restrictions induced by particle size confinement prevents a complete assignment of the structure of the Ce-50 to Ce-00 samples at this point.

Conclusion

We have demonstrated a simple and effective way to synthesize a complete range of $Ce_{1-x}Zr_xO_2$ nanoparticle sols ($x = 0-1$). The resultant sols are transparent and highly stable and exhibit a narrow particle size distribution. The average particle size for pure CeO_2 nanoparticles is about 2.5 nm. XRD studies show that all of the samples except the pure ZrO_2 and the Ce-10 sample are well crystalline. This is confirmed by HRTEM measurements showing highly crystalline, defect-free nanoparticles. XRD as well as Raman studies prove the formation of solid solutions between ceria and zirconia.

Experimental Section

Materials. Ammonium cerium nitrate, $(NH_4)_2Ce(NO_3)_6$ (Aldrich, 98.5%), zirconyl chloride, $ZrOCl_2 \cdot 8H_2O$ (Riedel-de Haën, 99.5%), ammonia, NH_3 (Fluka, 25%, aqueous solution), and nitric acid, HNO_3 (Aldrich, 90%), were used as received.

Synthesis. $Ce_{1-x}Zr_xO_2$ nanoparticle sols with $x = 0$, 0.1, 0.2, 0.3, ..., 1 were synthesized. For the synthesis of the sols with a total metal content of 0.005 mol, the appropriate amounts of $(NH_4)_2Ce(NO_3)_6$ and $ZrOCl_2 \cdot 8H_2O$ were dissolved together in 40 mL of distilled water. A total of 1.3−1.5 mL of a 25% aqueous NH_3 solution was added rapidly to this solution to raise the pH above 10, leading to coprecipitation of the metal hydroxides. The precipitate was washed repeatedly with

(37) Tosan, J. L.; Durand, B.; Roubin, M.; Bertin, F.; Loiseleur, H. *Eur. J. Solid State Inorg. Chem.* **1993**, *30*, 179−193.
(38) Spanier, J. E.; Robinson, R. D.; Zheng, F.; Chan, S. W.; Herman, I. P. *Phys. Rev. B* **2001**, *64*.
(39) Richter, H.; Wang, Z. P.; Ley, L. *Solid State Commun.* **1981**, *39*, 625−629.
(40) Southon, P. D.; Bartlett, J. R.; Woolfrey, J. L.; Ben-Nissan, B. *Chem. Mater.* **2002**, *14*, 4313−4319.
(41) Wachs, I. E. *Catal. Today* **1996**, *27*, 437−455.

distilled water until the washing was tested neutral by litmus paper. A total of 5 mL of distilled water and a calculated amount of 90% HNO_3 were added to the washed precipitate. The ratio of HNO_3−metal content was varied systematically from 1:1 for a pure CeO_2 sample to 1.5:1 for a pure ZrO_2 sample. The resultant suspension was sonicated (Elma Transsonic Digital S, 140% ultrasound power) for 45−60 min to obtain a transparent sol. During sonication, the temperature of the water bath increased to 40−50 °C. The pH of these sols was below 2. The sols were dialyzed against Millipore water using Spectra/Por membranes (MWCO: 6−8000). The pH of the dialyzed sols was in the range of 4−5. Transparent gels were obtained from these sols upon evaporation of water. The particle size distribution was studied for pure CeO_2 and pure ZrO_2 sols using a Beckman Optima XL-I analytical ultracentrifuge (Beckman Instruments, Palo Alto, CA) equipped with Rayleigh interference and UV absorption optics. A CM200FEG (Philips) microscope, operated at 200 kV, equipped with a field emission gun was used for HRTEM and SAED studies of the sols. Dried and powdered gels were used for XRD and Raman spectroscopy studies. A D8 advance diffractometer (Bruker AXS) with Cu Kα radiation obtained using a Ni/C mirror was used to obtain XRD data of all of the samples. All Raman spectra were recorded with a DILOR LABRAM 1 spectrometer. A He laser (632.8 nm, Melles Griot, 17 mW) was used for excitation. The laser light was focused onto the sample using a 10× objective lens (Olympus), and the spectra were recorded in backscattering geometry. The laser power at the sample location was measured and found to be less than 1 mW. The entrance slit was set to 100 μm, giving a spectral width of 5 cm^{-1}. A notch filter was applied to cut off the laser line and the Rayleigh scattering up to about 150 cm^{-1}. Each spectrum is the average of five accumulations at an integration time of 60 s.

Acknowledgment. Financial support by the Max-Planck-Society and the International Max Planck Research School (IMPRS) on biomimetic systems is gratefully acknowledged. We thank Antje Völkel for the AUC measurements and Dr. Helmut Cölfen for helpful discussions. We thank the Fritz-Haber-Institute and Prof. R. Schlögl for the use of the electron microscope and Klaus Weiss for technical assistance.

CM040155W